



Cite this: *Analyst*, 2019, **144**, 3398

Analytical performance of μ -groove silicon attenuated total reflection waveguides

Julian Haas, ^a Anja Müller,^b Lorenz Sykora^b and Boris Mizaikoff ^{*a}

The analytical performance of micromachined μ -groove silicon attenuated total reflection (ATR) elements has been evaluated in a comparison of Fourier-transform infrared (FTIR) and quantum cascade laser (QCL) spectroscopy operating at mid-infrared (MIR) wavelengths. μ -Groove silicon ATR elements are highly efficient micromachined waveguides fabricated at a wafer scale at such low cost that they may be considered a consumable for single-time-use, e.g., in medical application scenarios. Herein, exemplary analytes have been used for reliably evaluating their analytical performance (*i.e.*, acetate and carbonate) in terms of sensitivity, noise level, and achievable limits of detection in a comparison of broadband vs. narrowband infrared spectroscopy.

Received 5th March 2019,
Accepted 30th March 2019

DOI: 10.1039/c9an00417c

rscl.li/analyst

Introduction

Spectroscopy in the mid infrared (MIR) spectral region, extending from approximately 2.5 μm to 25 μm (4000 cm^{-1} to 400 cm^{-1}) has readily matured as a routinely deployed analytical method. In the MIR, well pronounced fundamental vibrational, rotational and roto-vibrational modes are accessible, dependent on investigating gaseous or condensed phase analytes. Besides pure qualitative analysis, quantitatively information is further accessible *via* the Beer–Lamberts-Law in absorbance or transmittance experiments. However, since virtually all organic and inorganic materials have excitable transitions in the MIR, instrumentation can potentially be demanding. Especially, attenuated total reflection (ATR) based experiments impose high demands on the internal reflection elements (IRE). Conventionally, rather bulky and expensive materials and crystals thereof are required for infrared spectroscopy since MIR transparent materials are rather rare. On the one hand, ATR enables spectroscopy on IR opaque analytes and analyte matrices such as polymers or aqueous solutions. Thin films that are required for transmission experiments are rather fragile and difficult to handle, while liquid cells for MIR spectroscopy require MIR transparent window materials, too. ATR spectroscopy is based on guiding light within an IRE and light/analyte interaction *via* the evanescent field. Commonly, IREs (mainly hemispheres, prisms and trapezoids) are made of zinc selenide (ZnSe), zinc sulfide (ZnS), germanium (Ge) or diamond due to the adequate MIR transparency, high refrac-

tive indices and resilience towards the samples. Selecting the best suited IRE materials as well as the right, commercially available, accessory, can be highly non trivial since, both, accessory and ATR element may have their very own advantages and disadvantages.¹ Robustness, sensitivity, compatibility to the equipment and the planned sensing task as well as cost have to be taken into account. In this context, reducing the physical dimension of the IRE and moving to less expensive materials, while maintaining or even improving the analytical performance of ATR elements, are readily pursued. Micromachined silicon (Si) wafers have been recently introduced as cost-efficient and flexible alternative to bulk Si ATR elements.^{2,3} Such thin silicon wafers open up the spectral window below 1400 cm^{-1} that is not accessible by bulk Si elements due to low transmission.⁴ What is more, such silicon chips are readily modified with noble metals such as gold to enable surface enhanced (SEIRAS) approaches^{5–7} or hypenated techniques in combination with electrochemical analysis.⁸ In the context of reducing the food-print, quantum cascade lasers (QCLs) and tunable QCLs (tQCLs) have recently matured as a potential alternative to conventional FTIR spectroscopy. High spectral resolution capabilities, increasingly broader tuning ranges and high spectral power emission provide performance that potentially may surpass FTIR spectroscopy.^{9–12} While, in a first approach, transmission based experiments highly benefit from QCL technology, similar trends are observable for ATR experiments based on bulk IRE crystals as well as on waveguide technology.¹³ Thin films made of *e.g.* diamond, mercury-cadmium-telluride (HgTeCd, MCT) or gallium arsenide (GaAs) are readily used for chem/bio sensing tasks of *e.g.* proteins or environmentally relevant pollutants.^{14–23} Furthermore, fibre based approaches are increasingly available for sensing in the MIR.^{24–28} Given

^aInstitute of Analytical and Bioanalytical Chemistry, Ulm University,

Albert-Einstein-Allee 11, 89081 Ulm, Germany. E-mail: boris.mizaikoff@uni-ulm.de

^bWalter Schottky Institute, Technical University Munich, Am Coulombwall 4, Munich, Germany

such a broad variety of available technologies, devices and designs, comparing different techniques against each other *i.e.* with respect to the analytical performance and affiliating novel concepts into the existing canon can be challenging.¹ In the present study commercially available and routinely utilized ATR cells, the BioATR II and the ConcentratIR 2 were compared to micromachined μ -groove based Si wafer in a “basic” and “signal enhanced” chip modification²⁹ *via* a FTIR spectrometer. Additionally, coupling with a QCL based spectrometer setup is being evaluated.

Experimental

Materials

Potassium carbonate (K_2CO_3 , VWR International GmbH), sodium acetate (NaAc , CH_3COONa , VWR International GmbH), deionized water (DI, resistivity $18.2 \text{ M}\Omega \text{ cm}$ at $25 \text{ }^\circ\text{C}$, Millipore). Standard solutions of $0.5 \text{ g K}_2\text{CO}_3$ in 100 mL DI water and 10 g NaAc in 100 mL DI were prepared by weighting the respective salts and dissolving them subsequently. Dilution rows were prepared by subsequently diluting the standard solution with DI.

Fabrication of microfabricated μ -groove Si wafer chips

Micro structured Si (100) wafer chips were fabricated in a first step according to Schumacher *et al.*² V-shaped grooves were etched from the back side of the wafer with a wet chemical etching process based on KOH. The resulting chips were ready to use as “basic” chip variation. “Enhanced” chips were further structured from top side in a second step with a dry etching protocol based on reactive ion etching (RIE) process that resulted in the creation of micro pillars, according to ref. 30.

Instruments and software

A Bruker Vertex 70 FTIR spectrometer was used for the FTIR analysis. The spectrometer was equipped with a liquid nitrogen (LN_2) cooled wide-band MCT detector. Spectra were recorded within a spectral range from 600 cm^{-1} to 4000 cm^{-1} with a spectral resolution of 2 cm^{-1} averaging 128 scans each spectrum. All spectra were recorded *versus* a water background. Data recording was performed *via* OPUS spectroscopy software (Bruker Optics GmbH) and data evaluation was performed with eFTIR (Operant LLC). The different cells were mounted in the spectrometers sample compartment with the manufacturers QuickSnap baseplate which allowed quick switching in-between the cells. The “basic” μ -groove Si IREs (IRUBIS GmbH) were mounted within a Teflon based liquid cell with a volume of about $100 \mu\text{L}$ forming an inverse cone. The μ -grooves are aligned parallel to the light beam, in contrast to the usual ATR crystal alignment to increase in-coupling efficiency *via* the elongated groove sidewalls, as shown in Fig. 1a. In Fig. 1b, light propagation in the direction of propagation has been condensed, showing only the lateral light propagation, which closely resembles a conventional in-coupling

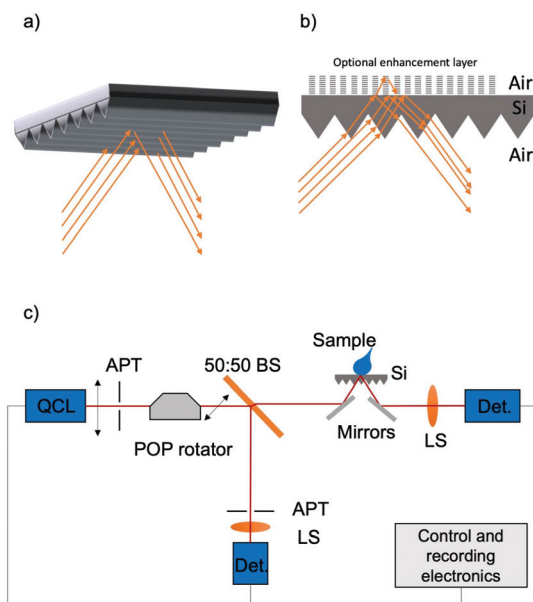


Fig. 1 (a) Schematic beam path of the three-dimensional alignment of the μ -grooves oriented parallel to the beam path, *i.e.* light incident from the left side of the scheme. (b) Simplified schematic beam path in 2-D through micromachined μ -groove silicon ATR elements with the optional enhancement layer, displayed *via* dashed pillars. For illustration, the three-dimensional in-coupling path has been reduced to two-dimensions by condensing the chip length. Hence, the chip expansion into the direction of light propagation has been simplified, showing only the lateral direction that resembles commonly utilized in-coupling by direct incidence on the prism flanks. (c) Schematic experimental setup of the QCL experiments comprising the QCL light source, beam shaping apertures (APT), ZnSe lenses (LS), the plane of polarization rotator (POP rotator), mirrors, the micromachined μ -groove silicon wafer, as well as a 50 : 50 ZnSe beam splitter (50 : 50 BS) and two detectors (Det.) and the control and recording electronics.

ling scheme *via* prism sidewalls. The sample cell for the micro-machined silicon chips uses a mirror to guide light towards the bottom side of the silicon the comprises of the in-coupling tranches. Light is totally internally reflected, coupled out of the chip and guided towards the detector *via* a second mirror. The top side of the silicon chips is either unstructured (“basic” chip) or micro structured (“signal enhanced”).

The BioATR II cell (Bruker Optics GmbH) consists of a $380 \mu\text{m}$ thick Si IRE/ATR element that is directly in contact with the sample volume in combination with a ZnSe focusing element and provides about seven to eight internal reflections. The whole cell consists of stainless steel and offers a sample tray that is completely filled with $50 \mu\text{L}$ of sample volume. The ConcentratIR2 cell (Harrick Scientific) uses the same coupling mechanism like the BioATR II cell. However, the disk-shaped silicon IRE/ATR element is exchanged with a $250 \mu\text{m}$ thick diamond disk that provides about ten internal reflections. Hence the diamond is in direct contact with the sample. Again, $50 \mu\text{L}$ of sample volume completely fill the sample tray of the cell. A MIRcat QCL (Daylight Solutions, Inc.) was deployed as light source for the QCL measurements. The laser

system consisted of four individual QCLs optically coupled to a single out-put port. The QCLs were operated in pulsed mode with a pulse length of 500 ns and a duty cycle of 5%. In summary, the QCL system provided $>100:1$ linear, vertically polarized radiation from 2000 cm^{-1} to 900 cm^{-1} . Tuning of the emission wavelength was performed in 2 cm^{-1} increments from 1200 cm^{-1} to 1900 cm^{-1} since the plane of polarization (POP) rotator limited the transmission range below 1200 cm^{-1} . Rotation of the POP was performed with a broadband achromatic POP rotator (Innovation Photonics), so that the radiation was horizontally polarized after passing the optical component. Subsequently light was passed through a 50:50 ZnSe beam splitter. Half of the radiation was fed into the micro-machined silicon wafer with aluminium mirrors and subsequently focused with a ZnSe lens on a thermoelectrically (TEC) cooled MCT detector (Vigo Systems). The other half of the beam was directly focused with another ZnSe lens on another TEC cooled MCT detector (Vigo Systems). Electrical signals of both detectors were acquired and digitized with a 14-Bit Digitizer (National Instruments, NI 9775) via a Labview script (National Instruments, Labview 2017). Data treatment and evaluation was performed with Origin 2017 (OriginLab). Spectra for each calibration point, *i.e.* each concentration for each cell, was performed with five repetitions.

Results and discussion

Performance evaluation via FTIR

For comparing the analytical performance of two different commercially available cells with the micromachined Si wafers with a routine FTIR spectrometer, stable solutions of potassium carbonate, *i.e.* carbonate, CO_3^{2-} and sodium acetate, *i.e.* acetate CH_3COO^- , ions were used to provide reproducible measurement conditions. Furthermore, the ions were selected to provide simple and exemplary analytes for inorganic and organic molecules with well pronounced MIR signatures, *i.e.* strong bands. Acetate reveals two strong MIR transitions located at 1550 cm^{-1} and 1413 cm^{-1} . What is more, spectral bands of proteins (amide I and II), that are relevant for a wide palette of medical diagnostics, such as evaluation of protein misfolding in the context of neurodegenerative diseases, are located within this spectral region. Both bands of the acetate molecule are distinguishable from liquid water absorption. Exemplary spectra of a 100 mg mL^{-1} aqueous acetate solution, recorded with the four different cells are shown in Fig. 2. Whereas the band intensity of the BioATRII, the ConcentratIR2 and the signal enhanced chip appear to be in the same order of magnitude, the basic chip shows less pronounced band intensities. Furthermore, the BioATRII cell, that is based on a Si IRE shows significantly increased noise towards the longer wavelength region that can be attributed to the lower transmission through the Si IRE. On the contrary, the spectral window of the ConcentratIR2, that is equipped with a diamond IRE, is limited at the short wavelength regime above about 2000 cm^{-1} due to the diamond inherent two-phonon

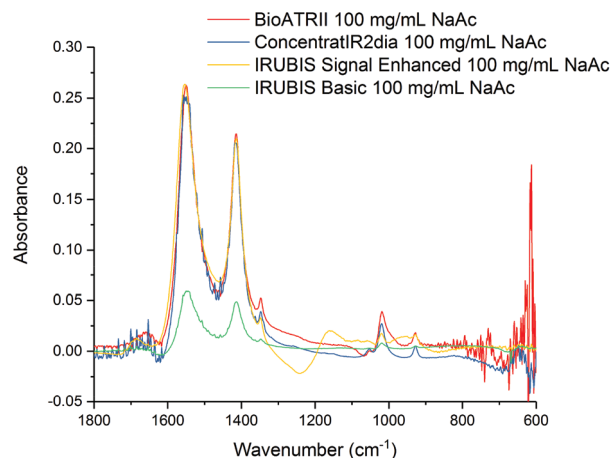


Fig. 2 Acetate MIR spectra (fingerprint region) of the four different sample cells vs. a water background. BioATRII (red line), ConcentratIR (blue line) and the signal enhanced micromachined Si wafer (yellow line) reveal comparable band intensities.

transition that limits the transmission within about 2000 cm^{-1} to 2600 cm^{-1} in the MIR.

Carbonate possesses a well pronounced band at 1390 cm^{-1} (Fig. 3). Again, band intensity of the ATR spectra that were recorded with the BioATRII, ConcentratIR2 and the signal enhanced chip are comparable while the basic configuration reveals a lower band intensity. Furthermore, noise levels are significantly increased towards the lower wavelength region $>900\text{ cm}^{-1}$ for the BioATRII spectra.

To evaluate the analytical figures of merit, such as sensitivity, noise levels as well as the effectivity, spectra of the prepared dilution rows were recorded with the different measure-

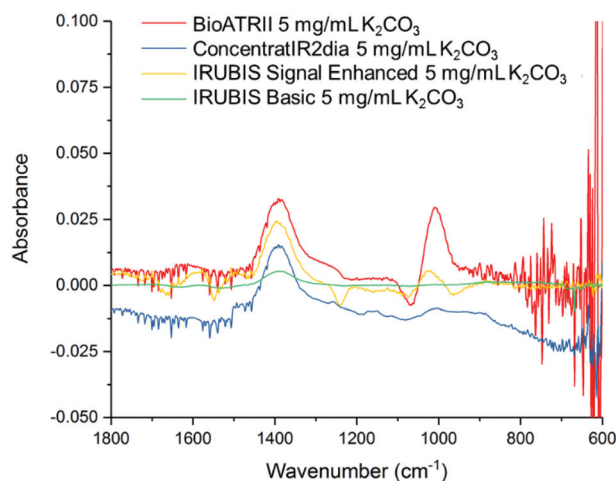


Fig. 3 Carbonate MIR spectra (fingerprint region) of the four different sample cells vs. a water background. The BioATRII (red line), ConcentratIR (blue line) and the signal enhanced micromachined Si wafer (yellow line) reveal comparable band intensities. Increased noise towards to long wavelength region is especially visible for the BioATRII equipped with a Si IRE.

ment cells while keeping the experiment parameters constant. Exemplary spectra of the calibration solutions with the basic Si chip are plotted in Fig. 4. Since the more pronounced acetate band at 1550 cm^{-1} is affected by the transition of liquid water that is centred at about 1640 cm^{-1} as well as by artefacts of atmospheric water vapour, the band at 1413 cm^{-1} was chosen for calibration and the band area was integrated from 1458 cm^{-1} to 1366 cm^{-1} . For evaluation of the performance for carbonate ions, the band at 1390 cm^{-1} was selected and integration was performed from 1465 cm^{-1} to 1310 cm^{-1} .

The signal enhanced Si wafer provides MIR bands that are more pronounced by a factor of about four when compared to the basic version (Fig. 5). Again, the spectral window is extended to the long wavelength region in comparison to the BioATR II cell due to a shorter path within the bulk silicon. However, silicon IREs have the inherent drawback of forming a native thin surface oxide layer. This silicon dioxide (SiO_2) layer

shows a band in the MIR around 1200 cm^{-1} , which is increasingly pronounced with an increased portion of the silicon surface area in contact with ambient air. Within a narrow spectral window of about 50 cm^{-1} around the SiO_2 band, any analytical signal response may be slightly affected. This effect is of course amplified for the signal enhanced chips since the enhancement layer provides an increased surface area. In contrast, diamond IREs are not affected by that feature.

For directly comparing the different ATR cells, integration of the selected bands was performed for all spectra of all cells and both analytes. Calibration curves for carbonate and acetate are shown in Fig. 6 and 7 respectively.

First, sensitivity of the different cells was derived from the slope of the line of best fit to the individual calibration points. Furthermore, noise was derived by integration of the absolute value of the baseline of the respective spectral area of the integrated bands. Furthermore, effectivity was calculated. Effectivity was calculated according to $\text{Effectivity} = \text{Sensitivity}/\text{Noise}$, which results in a performance indicator that directly

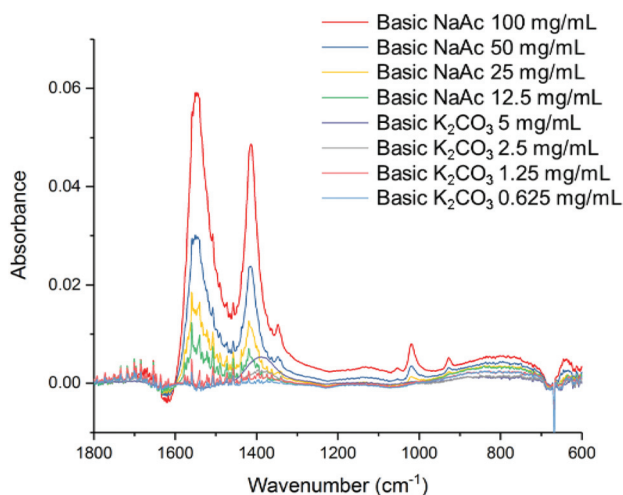


Fig. 4 Exemplary MIR calibration spectra of acetate and carbonate solutions, recorded with the basic chip (vs. water background) via FTIR.

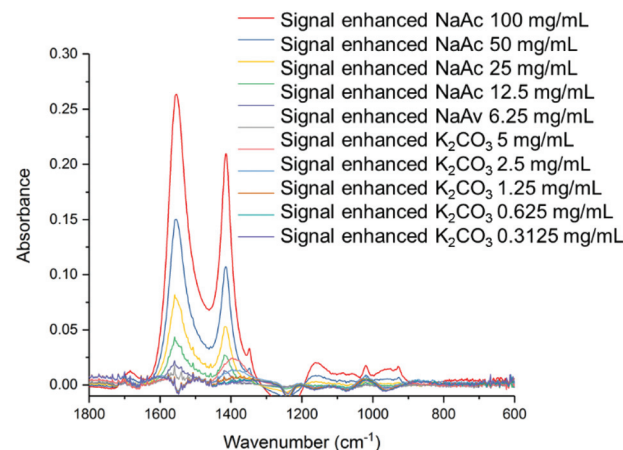


Fig. 5 Exemplary MIR calibration spectra of acetate and carbonate, recorded with the signal enhanced chip (vs. water background) via FTIR.

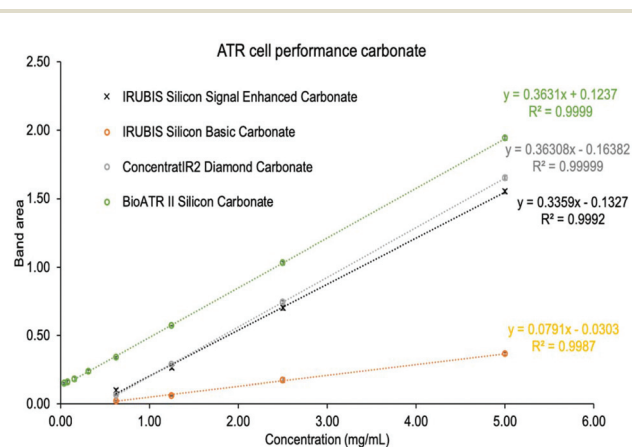


Fig. 6 Carbonate calibration for the four cells – integration was performed from 1465 cm^{-1} to 1310 cm^{-1} .

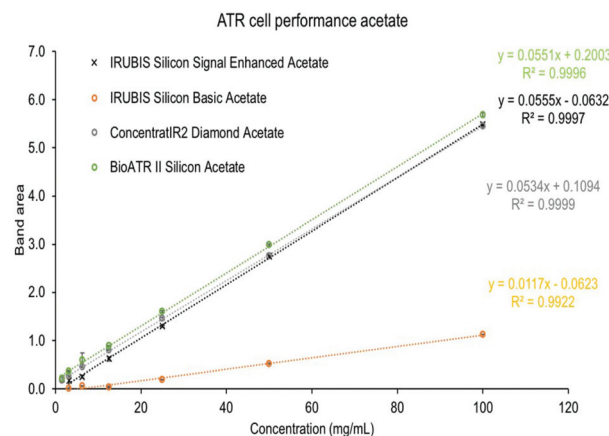


Fig. 7 Acetate calibration for the four cells – integration was performed from 1458 cm^{-1} to 1366 cm^{-1} .

Table 1 Comparison of the different ATR cells for carbonate at acetate detection. For comparing the performance, the table is arranged with respect to effectivity

	Sensitivity	Noise	Effectivity	LOD (mg mL ⁻¹)	LOQ (mg mL ⁻¹)
ConcentratIR2 diamond carbonate	0.3631	0.0656	5.5333	1	2
IRUBIS silicon basic carbonate	0.0791	0.0215	3.6654	1	3
IRUBIS silicon signal enhanced carbonate	0.3359	0.0989	3.3963	1	3
BioATR II silicon carbonate	0.3631	0.1500	2.4203	1	4
IRUBIS silicon basic acetate	0.0117	0.0103	1.1271	8	13
IRUBIS silicon signal enhanced acetate	0.0555	0.1653	0.3356	10	28
ConcentratIR2 diamond acetate	0.0534	0.1827	0.2921	8	29
BioATR II silicon acetate	0.0551	0.2140	0.2574	8	31

Table 2 FTIR ATR performance comparison of the basic vs. the enhanced version of the micromachine μ -groove Si chips

Sensitivity	
Signal enhanced/basic carbonate	4.2
Signal enhanced/basic acetate	4.7
Noise	
Signal enhanced/basic carbonate	4.6
Signal enhanced/basic acetate	15.9
Effectivity	
Signal enhanced/basic carbonate	0.9
Signal enhanced/basic acetate	0.3

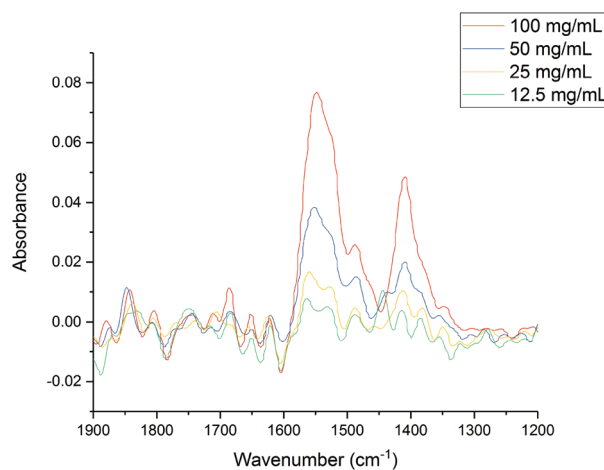
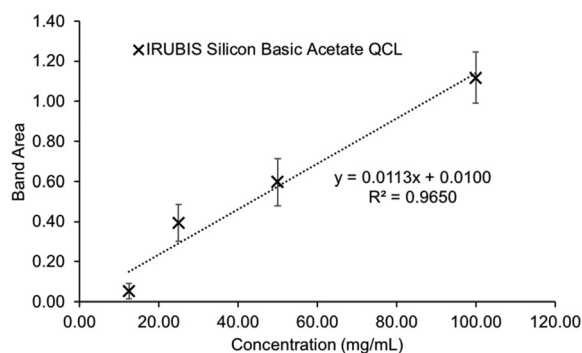
correlates the achievable sensitivity with noise levels.³¹ The limit of detection (LOD) was derived by the three-sigma criterion and the limit of quantification (LOQ) was derived from the 9-sigma criterion. The retrieved results are summed up in Table 1. Calculated LODs and LOQs are virtually identical for the four evaluated sampling cells.

In Table 2 the basic and the signal enhanced variations of the micromachined Si wafer are directly compared with respect to sensitivity, noise and effectivity. While sensitivity of the signal enhanced version is improved by a factor of about 4, noise is increased, too, which is due to the interference based enhancement mechanism.³² By comparing the noise response for carbonate detection, a factor similar to the sensitivity enhancement is retrieved, which leads to an effectivity of close to one. For acetate detection noise is increased by a factor of about 16 when comparing signal enhanced and basic version. Hence, effectivity is reduced to 1/3. In summary, the signal enhanced version improves band intensity, however, at the cost of increased noise levels. Hence, different concentrations are better distinguishable for the signal enhanced, yet, the basic version enables detection of lower quantities.

QCL based spectroscopy

Given the results obtained *via* FTIR spectroscopy, the basic micromachined Si chip was coupled to a QCL based MIR spectroscopy setup and the performance for detection of dissolved acetate in water was evaluated. Exemplary spectra are shown in Fig. 8 for four different concentrations of sodium acetate.

Again, band area from 1458 cm⁻¹ to 1366 cm⁻¹ was integrated to establish a calibration curve for the acetate response *via* the basic Si chip with a QCL based setup (Fig. 9). For the QCL based analytical figures of merit a sensitivity of 0.0113

**Fig. 8** QCL spectra of acetate in water recorded with the "basic" chip.**Fig. 9** Calibration of acetate in water with the "basic" chip – integrating the band from 1458 cm⁻¹ to 1366 cm⁻¹.

and a noise level of 0.01 was derived, leading to a LOD of 2 mg mL⁻¹. Both, sensitivity and noise level are virtually equal to FTIR spectroscopy-based evaluation. However, error bars of the individual calibration points are increased. This increased uncertainty can be explained by the inverse cone shape that exposed an increased surface area of the solutions to air. Hence, an increased amount of water evaporates during step-wise tuning of the QCL emission wavelength that can be reduced with a more sophisticated closed cell design.

Conclusion

The analytical performance of low-cost, potentially single use, micromachined μ -groove Si wafer chips has been evaluated in comparison to commercial, excessively used ATR cells for FTIR spectroscopy in the MIR. Limits of detection in the single-digit mg mL^{-1} were derived for the micromachined μ -groove Si wafer chips. Due to the low fabrication costs and readily available high-quality silicon, mass production for single-use application, while maintaining analytical performance of more elaborate sampling cells can be achieved. Furthermore, incorporation of the micromachined μ -groove Si chips into a QCL based spectroscopy setup has been evaluated. The evaluated spectral region is of high interest for chem/bio sampling in a medical context. Given the high spectral energy density of tunable QCLs, multiplexed concepts can be further envisioned, also for a single laser light source. The herein deployed reference arm of the divided beam may be used for parallel sensing concepts with further sampling cells, even with further levels of beam splitting, a.k.a. a higher level of integration. Given the rapid progress in chemometrics and multivariate statistics, such concepts can potentially benefit for evaluation in individual spectral data or for correlating information retrieved from multiple cells.

Funding

This study has in part been funded by the H2020-ICT-2016–2017 project MIRACLE (#780598) funded by the European Union and has in part been funded by the Medical Valley Award 2017 project ATR Biofluide funded by the Bavarian Ministry of Economic Affairs, Energy and Technology.

Author contributions

All authors have given approval to the final version of the manuscript.

Conflicts of interest

Lorenz Sykora and Anja Müller are shareholders of IRUBIS GmbH.

References

- 1 T. Schädle and B. Mizaikoff, *Appl. Spectrosc.*, 2016, **70**, 1072–1079.
- 2 H. Schumacher, U. Künzelmann, B. Vasilev, K.-J. Eichhorn and J. W. Bartha, *Appl. Spectrosc.*, 2010, **64**, 1022–1027.
- 3 E. Karabudak, B. L. Mojjet, S. Schlautmann, G. Mul and H. J. G. E. Gardeniers, *Anal. Chem.*, 2012, **84**, 3132–3137.
- 4 T. A. Morhart, S. Read, G. Wells, M. Jacobs, S. M. Rosendahl, S. Achenbach and I. J. Burgess, *Appl. Spectrosc.*, 2018, **72**, 1781–1789.
- 5 J. Srajer, A. Schwaighofer, G. Ramer, S. Rotter, B. Guenay, A. Kriegner, W. Knoll, B. Lendl and C. Nowak, *Nanoscale*, 2014, **6**, 127–131.
- 6 V. Nedelkovski, A. Schwaighofer, C. A. Wraight, C. Nowak and R. L. C. Naumann, *J. Phys. Chem. C*, 2013, **117**, 16357–16363.
- 7 I. R. Andvaag, T. A. Morhart, O. J. R. Clarke and I. J. Burgess, *ACS Appl. Nano Mater.*, 2019, **2**, 1274–1284.
- 8 T. A. Morhart, B. Unni, M. J. Lardner and I. J. Burgess, *Anal. Chem.*, 2017, **89**, 11818–11824.
- 9 A. Schwaighofer, M. Montemurro, S. Freitag, C. Kristament, M. J. Culzoni and B. Lendl, *Anal. Chem.*, 2018, **90**, 7072–7079.
- 10 M. R. Alcaráz, A. Schwaighofer, C. Kristament, G. Ramer, M. Brandstetter, H. Goicoechea and B. Lendl, *Anal. Chem.*, 2015, **87**, 6980–6987.
- 11 A. Schwaighofer, J. Kuligowski, G. Quintás, H. K. Mayer and B. Lendl, *Food Chem.*, 2018, **252**, 22–27.
- 12 A. Schwaighofer, M. R. Alcaráz, C. Araman, H. Goicoechea and B. Lendl, *Sci. Rep.*, 2016, **6**, 33556.
- 13 T. Schädle and B. Mizaikoff, *Appl. Spectrosc.*, 2016, **70**, 1625–1638.
- 14 M. Sieger, J. Haas, M. Jetter, P. Michler, M. Godejohann and B. Mizaikoff, *Anal. Chem.*, 2016, **88**, 2558–2562.
- 15 J. Haas, R. Stach, M. Sieger, Z. Gashi, M. Godejohann and B. Mizaikoff, *Anal. Methods*, 2016, **8**, 6602–6606.
- 16 P. Piron, E. Vargas Catalan, F. Nikolajeff, L. Österlund, P. O. Andersson, J. Bergström, M. Karlsson, J. Haas and B. Mizaikoff, in *Photonic Instrumentation Engineering V*, ed. Y. G. Soskind, SPIE, 2018, p. 15.
- 17 J. Haas, E. V. Catalán, P. Piron, F. Nikolajeff, L. Österlund, M. Karlsson and B. Mizaikoff, *ACS Omega*, 2018, **3**, 6190–6198.
- 18 X. Wang, S.-S. Kim, R. Roßbach, M. Jetter, P. Michler and B. Mizaikoff, *Analyst*, 2012, **137**, 2322.
- 19 B. Mizaikoff, X. Wang, M. Sieger, L. Faraone, J. Antoszewski, W. Lei, M. Jetter and P. Michler, in 2014 Conference on Optoelectronic and Microelectronic Materials & Devices, IEEE, 2014, pp. 301–302.
- 20 Á. I. López-Lorente, P. Wang, M. Sieger, E. Vargas Catalan, M. Karlsson, F. Nikolajeff, L. Österlund and B. Mizaikoff, *Phys. Status Solidi*, 2016, **213**, 2117–2123.
- 21 M. Sieger, F. Balluff, X. Wang, S. Kim, L. Leidner, G. Gauglitz and B. Mizaikoff, *Anal. Chem.*, 2013, **85**, 3050–3052.
- 22 X. Wang, M. Sieger and B. Mizaikoff, in *Quantum Sensing and Nanophotonic Devices X*, ed. M. Razeghi, SPIE, 2013, p. 86312M.
- 23 X. Wang, M. Karlsson, P. Forsberg, M. Sieger, F. Nikolajeff, L. Österlund and B. Mizaikoff, *Anal. Chem.*, 2014, **86**, 8136–8141.
- 24 T. Lewi and A. Katzir, *Opt. Lett.*, 2012, **37**, 2733.

- 25 T. Schädle, A. Eifert, C. Kranz, Y. Raichlin, A. Katzir and B. Mizaikoff, *Appl. Spectrosc.*, 2013, **67**, 1057–1063.
- 26 R. Lu, G. Sheng, W. Li, H. Yu, Y. Raichlin, A. Katzir and B. Mizaikoff, *Angew. Chem., Int. Ed.*, 2013, **52**, 2265–2268.
- 27 V. K. Katukuri, J. Hargrove, S. J. Miller, K. Rahal, J. Y. Kao, R. Wolters, E. M. Zimmermann and T. D. Wang, *Biomed. Opt. Express*, 2010, **1**, 1014.
- 28 P. Hahn, M. Tacke, M. Jakusch, B. Mizaikoff, O. Spector and A. Katzir, *Appl. Spectrosc.*, 2001, **55**, 39–43.
- 29 L. Sykora, DE102015011687 A1, 2015.
- 30 L. Sykora, WO2017/045998 A1, 2017.
- 31 T. Schädle and B. Mizaikoff, *Appl. Spectrosc.*, 2016, 1–8.
- 32 P. Huber-Wälchli and H. H. Günthard, *Spectrochim. Acta, Part A*, 1978, **34**, 1253–1262.